SPE
Society of Petroleum Engineers

SPE 23970

Three-Dimensional Conditional Simulation of Schneider (Buda) Field, Wood County, Texas

R.D. Ravnaas* and R.F. Strickland,* Cawley, Gillespie & Assocs.; L.W. Lake,* U. of Texas; A.P. Yang,* Texaco E&P Technology Div.; Mohammad Malik, U. of Texas; D.R. Prezbindowski, International Petrology Research; and Tom Mairs, Consulting Geologist

*SPE Members

This paper was prepared for presentation at the 1992 SPE Permian Basin Oil and Gas Recovery Conference held in Midland, Texas, March 18–20, 1992.

Abstract

A three dimensional conditional simulation model, integrating a comprehensive data base coupled with engineering, geological, and petrological studies, has significantly enhanced reservoir management capabilities in the Schneider (Buda) Field. Presented are the results of a series of conditional simulations of the Schneider (Buda) Field. The Schneider (Buda) Field is developed in a Buda reef complex. Porosity types change significantly between reservoir facies. A three dimensional conditional simulation generated using only well control points did not adequately characterize the reservoir. An intermediate two dimensional conditional simulation using additional assumptions was then generated to refine and control the final three dimensional conditional simulation. The resulting three dimensional conditional simulation delineates permeability distributions that better: 1) represent the calculated heterogeneity, 2) match the available core data, and 3) model the geologic characterization including the defined facies. The resulting distributions have been applied to a three dimensional fluid flow simulation to better predict fluid movement through the reservoir.

References and figures at end of paper

Introduction

The Schneider (Buda) Field is located in Wood County, Texas, approximately 100 miles east of Dallas near the town of Hainesville (Figure 1). Production is from Cretaceous reefal Buda Limestone discovered under the overhang of the Hainesville salt dome (Figure 2). Bounded by faults to the east and west, the updip limit is the salt dome, and the downdip limit is a tar mat/water contact. Originally a depletion drive black oil reservoir, it was undersaturated at discovery. The field was discovered by the Dan Peacock No. 1 well flowing 1,008 BOPD with a 1,000 psi flowing tubing pressure from perforations at 9,400 feet on March 4, 1988 (Figure 3). The field was unitized and a water injection project initiated in October, 1990, with three producing wells and one injection well.

Production/Injection History

Production began in the Schneider (Buda) Field in March, 1988, with the discovery well, the Peacock No. 1. Four wells have been drilled in the field with the discovery well converted to injection in October, 1990. As of August 31, 1991, cumulative production from the field was 1,286 MSTB with recent production rates averaging a total of 1,500 BOPD for the current three producing wells (Figure 4). Cumulative water injection as of August 31, 1991, was

687 MSTB with recent injection rates in the Peacock No. 1 averaging 2,400 BWIPD. The cumulative injection/ withdrawal ratio since October, 1990, is 1.3.

Pressure History

The original reservoir pressure at -9,022 feet subsea was 4,090 psia (Figure 5). This black oil reservoir was undersaturated by 765 psi with an original bubble point pressure of 3,325 psia. Bottomhole pressures were taken when each well was initially completed and then on a regular, quarterly basis. The reservoir pressure fell quickly until the bubble point pressure was reached in early 1989. Production rates were voluntarily restricted to 300 BOPD per well to preserve reservoir energy until the field was unitized and water injection initiated.

A relatively inexpensive but useful interference test was conducted when injection began in October, 1991. The Peacock No. 1, Jones No. 2, and Jones No. 3 STH wells have extremely high flow capacity and reach average reservoir pressure in less than 24 hours of shut-in. Baseline static pressures were obtained in all three wells with Amerada gauges just prior to injection in the Peacock No 1. The pressures were in close agreement and averaged 2,910 psia. Thereafter, on a weekly basis, the wells were shut-in overnight and bottomhole static pressures were obtained. Pressure response due to injection was measured on both the Jones No. 2 and Jones No. 3 STH after two weeks of injection. Pressures were recorded weekly for several months. This pressure information has proven invaluable to properly match the interwell reservoir flow capacity in the fluid flow simulator.

Fluid Properties

A bottomhole fluid sample was obtained during the completion of the Peacock No. 1. Bottomhole temperatures have been recorded in the Peacock along with other wells in the Hainesville Dome area. The temperature gradient is typical of the area[1] and the temperature at the reservoir datum of -9,022 feet subsea is estimated to be 215 degrees F. The bubble point pressure was calculated to be 3,325 psia at 215 degrees F. The subsequent pressure history from the field demonstrated good agreement with the predicted bubble point, as indicated by the pressure-cumulative production plot leveling off as pressures fell below 3,325 psia. Combination fluid properties[2,3] were calculated from differential liberation and separator tests for input to the black oil simulator. The original oil formation volume factor was 1.305 RB/STB corrected to field separator conditions. The original solution gas/oil ratio was 565 SCF/STB, and the oil viscosity was 0.93 cp. Stock tank oil gravity is approximately 26 degrees API.

Core Acquisition/Petrophysical Properties

Every well in the reservoir was conventionally cored for a total of 445 feet of core material. Full diameter whole core analysis was performed on the cores taken from the heart of the reef, the Jones No. 2 and Jones No. 3 STH. Kmax, K90 and Kvert were measured. Plug analysis was performed on the Peacock No. 1 and the SASI Ranch No. 1. Full diameter analysis was performed on selected intervals in the reef debris facies of the Peacock. Helium was used for all porosity measurements. The net pay arithmetic average core permeability is 65 md. Inspection of the core plus knowledge of the size of the vugs typically present in reef facies suggest that even the whole core measured permeabilities are lower than true, in-situ permeabilities. Pressure transient tests and history matching of the injection interference pressures confirm this observation.

A full suite of open hole well logs was run in every well, including neutron, density, and sonic logs. Equations were developed relating core porosity to the porosity log readings to estimate porosity in intervals of missing core data. Average net pay porosities vary from well to well from a high in the Peacock of 15.7 percent to a low in the SASI Ranch of 10.0.

Numerous special core tests were conducted, including steady state water-oil relative permeability, waterflood displacement, unsteady state gas/oil relative permeability, air-brine drainage centrifuge capillary pressure, brine-oil imbibition centrifuge capillary pressure, and centrifuge gas-oil relative permeability. Electrical properties (m and n tests) plus formation compressibility were measured. As expected, rock compressibility was greater in the reefal and reef debris facies than in the grainstone shoal.

Geological and Petrological Studies

All core material from the four wells (SASI Ranch, Peacock, Jones 2 and Jones 3 STH) were studied from the

Schneider Field in order to establish controls on reservoir development. Detailed descriptions of the cores were prepared noting lithology, sedimentary structures, porosity, grain types and petrophysical signature. A detailed petrographic study was also carried out using transmitted light and scanning electron microscopy. The purposes of this study were to: 1) document the type, size and distribution of porosity in the Schneider Field; 2) determine the origin of the porosity, its relationship to depositional facies, and controls on reservoir heterogeneity, and 3) develop a reservoir model that will allow the reliable projection of reservoir quality beyond the well bore (Figure 6).

Geological Reservoir Model

The Schneider Field reservoir is developed in a Buda (Lower Cretaceous) marine reef complex limestone. This reef complex grew on the south flank of a paleotopographic high formed during an early stage of salt movement. Salt movement (diapirism) has been demonstrated to be a control for reef and grainstone shoal distribution in the East Texas Basin.[4] Reefal organisms provide the source for skeletal grains within the shoal complex. Lithofacies distribution indicates that the present Buda structure generally represents an exaggerated model of paleodepositional topography. The development of higher energy reef, reef apron carbonate sands and fore-reef/shoal debris facies on the deeper water carbonate mudstones and wackestones documents a shallowing upwards sequence. Subaerial exposure terminated the development of Schneider reef complex and enhanced reservoir quality by meteoric water leaching.

Four major limestone lithofacies are recognized in the Schneider reef complex. The productive reservoir lithofacies are: reef debris, reef, and shoaling grainstone apron (Figures 7, 8, and 9). The fourth lithofacies, a pre-reef limestone, is not considered productive. These lithofacies developed in a vertical and off-structure direction. Reservoir porosity distribution is controlled by depositional facies, early diagenesis and bitumen distribution.

Three major types of porosity (affecting reservoir characteristics) are present in the Schneider Field: 1) skelmoldic porosity (formed shortly after deposition by selective dissolution of skeletal grains, particularly corals); 2) primary interparticle porosity (formed at the time of deposition); and 3) micro-fracture porosity (formed during burial and associated with stresses generated during salt movement). Porosity types change and reservoir quality decreases down section and down dip.

Solid hydrocarbons (bitumen) also seriously degrade the reservoir quality in the lower portions of the Schneider Field. Overall degradation of reservoir quality by porosity plugging bitumen increases with depth, creating an asphalt seal at or near the oil/water contact. This asphalt seal is analogous to what is found in the nearby Hawkins Field.[5-7] Bitumen and pyro-bitumens can form by a number of different processes,[8] so the distribution of the bitumen within the reservoir offers clues to its origin. The occurrence of the solid hydrocarbon in the lower portion of the reservoir and in association with the major fault to the west indicates that water washing may be responsible for its development. Additional data is required to confirm this interpretation.

Reservoir Lithofacies

Pre-reef Limestones - This non-reservoir quality lithofacies is present in the base of the cored Buda Formation (Figure 10F). The importance of this lithofacies increases in a down dip direction. Skeletal wackestone is the dominate limestone lithology and interfingers with the overlying packstone-grainstones of the reef debris lithofacies. Skeletal grains include foraminifera, pelecypod, gastropod, echinoid and coral fragments. Stylolites and micro-fractures are common. These mud dominated carbonate sediments were deposited in a low energy (below wave base) marine environment. Porosity is poorly developed because of the abundance of carbonate mud and the common occurrence of bitumen filling moldic pores.

Reef Debris - This lithofacies is composed of a coarsening upwards sequence of nonsorted to poorly sorted packstones and grainstones interfingered with the mud dominated wackestones of the pre-reef facies (Figures 10C and 10D). Skeletal fragments consisting of large randomly oriented corals and stromatoporoids dominate the sediment. Other skeletal grains include mollusk (including Inoceramus), coral and echinoid fragments. This lithofacies interfingers with the basinward and underlying pre-reef limestones and up-dip reef facies.

Deposition of this lithofacies occurred to the front of the reef complex facies. Storm and gravity transport of

reef derived sediments into deeper water, basinward of the reef, is responsible for deposition. Continued reef development used the proximal reef debris deposits as a base for further basinward growth leading to an interfingering of the two lithofacies. Reef debris deposits are common and have been documented in recent and ancient carbonate systems.[9]

Porosity consists of early secondary grain moldic and primary pores. Reservoir quality is variable and tends to decrease with increasing carbonate mud matrix content. Permeability measurements may provide an inaccurate measure of the flow characteristics within this facies because of the presence of randomly oriented, very large skeletal components. These partially leached skeletal components and the surrounding lithified carbonate muds can exceed the size of the core sample. Permeability measurements can be misleading when single grains are larger than the core diameter.

Reef Facies - This lithofacies is characterized by thick coral/stromatoporoid boundstones with a patch quilt distribution of discontinuous wackestone, packstone and grainstone units (Figures 10A and 10B). In addition to coral, skeletal components include echinoid, mollusk (pelecypod and gastropod), stromatoporoid, algae and foraminifera. Carbonate mud matrix is commonly present having been deposited in the baffled areas between coral stromatoporoid colonies. Lithification of the mud matrix and the early leaching of the skeletal components (corals, stromatoporoids and mollusk) resulted in large vuggy and tubular pore spaces. Coral and stromatoporoid colonization and prolific growth on the south flank of the Hainesville paleotopographic high formed the main reef complex. Current, wave and biological erosion of the reef complex were the sources of the sediments for the basinward shoaling grainstones and reef debris lithofacies. Subaerial exposure terminated reef development.

Porosity consists of early secondary and primary pores. The large size and volumetric importance of leached skeletal components and sheltered pore primary pore spaces within this facies accounts for its overall excellent reservoir quality.

Shoaling Grainstone Apron - This lithofacies consists of skeletal grainstones developed to the front of the main patch reef complex by wave and current reworking of reef sediments (Figure 10E). Skeletal grains include broken and rounded fragments of mollusk, coral, stromatoporoid and echinoid fragments. The lithofacies thins and interfingers with underlying reef debris limestones and the down-dip pre-reef limestones. Harbour and Mathis[10] document a relationship between rudist reefal development and carbonate grainstone shoal development in Black Lake Field of central Louisiana. Reef and reef-derived skeletal grainstone facies have been documented for the Lower Cretaceous James Reef (Fairway Field) of East Texas.[11] In each of these systems, reefal organisms served as the grain source for the carbonate sands.

Porosity consists of secondary grain moldic and primary interparticle pore spaces. The energy of the depositional environment and the degree of early meteoric leaching controlled porosity development. Deposition down-dip occurred in lower energy marine environments (deeper water), which resulted in thinner grainstone beds and poorer sorting characteristics that rapidly reduced reservoir quality.

Conditional Simulation

There are several methods used to incorporate the geological reservoir model in the development of permeability and porosity distributions for input to fluid flow simulators.[12-16] Traditional contouring, whether by hand or computer mapping packages, of permeabilities and porosities, often understates the true heterogeneity of the reservoir. Hand contouring relies on the experience of the individual in mapping interwell properties. Most popular computer mapping packages use mathematical rules for interpolation without regard to the spatial statistics of the property. Since these types of contouring reflect only large scale variation, they do not account for fine scale property variation. In fluid displacement processes, one consequence of this reduction in modeled heterogeneity is to predict sweep efficiencies that are too high, giving optimistic forecasts.

When adequate data is available, application of geostatistical techniques defines the spatial relationships of the property.[17-25] Given the spatial relationships (autocovariance models), maps created by kriging can be constructed. Kriging gives the optimal (minimum variance) estimate of the property at every location. However, kriged maps, by themselves, also smooth the distribution, understating true heterogeneity. An enhancement to

kriging, referred to as "conditional simulation" has been devised to help account for fine scale property variations and maintain the actual heterogeneity of the reservoir.[19,26,27]

Conditional simulation is the process of constructing unsmoothed realizations, using geostatistical techniques, that honor the data at well control points (conditional). The steps in conditional simulation are:

1. Define an autocovariance model(s) based on the data obtained from the reservoir.

2. Krige a surface through the actual well control data.

3. Construct an unconditional realization using the autocovariance model. This realization does not honor data values at control point locations, but does simulate both large and fine scale variability that is similar to the actual distribution defined by the autocovariance model.

4. Krige a surface through the values obtained from the unconditional realization in step 3 using only those values at the actual well locations.

5. Subtract the kriged surface from the unconditional realization to obtain a residual field. This residual contains only small scale variations and, since the kriged surface uses the values at the control points, the residual at these locations is zero.

6. Add the residual from step 5 to the kriged surface of step 2. The resulting realization honors the well control points with heterogeneity comparable to the data obtained from the reservoir.

Application of Conditional Simulation

There are five basic steps to prepare for the conditional simulation procedure described above. See Yang[28] for more information.

Determine Probability Distribution

Most methods for testing probability distributions are for independent data and may not be suitable for data with strong spatial correlation. Because of this, visual inspection of the probability density function, pdf (or histogram) determines the proper type of distribution. The pdf is chosen because it offers both easy identification of symmetry and the presence of multiple peaks.

For the Schneider (Buda) Field, the pdf of the logarithm of permeability for each facies in the reservoir can best be approximated by normal distributions (the permeability is log normally distributed). The three reservoir facies show variations in the mean and variance. However, there is sufficient overlap on the pdf for the three facies so that the differences in the mean and variance are adequately reflected from the conditioning of the well data (step 2 above).

Variogram

A variogram is used to identify an autocovariance model. Log permeabilities were used because of greater precision and the observed log normal pdf. The variograms for each of the facies were linear and exhibited large fluctuations. Large fluctuations of the variogram indicate long-range spatial correlation because correlation reduces precision (increases fluctuations). A straight-line fit to the variogram implies a fractal model that does not level off as happens, for example, in a spherical model. Fractal models mathematically describe the complex shapes found in nature and have been used in a wide variety of geostatistical applications.[26,27,29-34]

R/S Plot

The slope of the rescaled range (R/S) plot[26,35,36] is used to determine the fractal exponent H of the fractal model. Even if the fractal model is not used, it is advisable to make an R/S plot to check the presence of long range correlation. Because the variogram is more precise when the separation distance is small, and the R/S plot is more precise when it is large, the R/S plot is more reliable in inferring long range correlation than the variogram which tends to under-estimate long range correlation.

There is no distinctive difference among the R/S plots of individual facies or wells in the Schneider (Buda) Field. Analysis of the plots results in an H= 0.85 for log permeability.

Autocovariance Model

Combining our observation of the pdf, variogram, and the R/S plot, the following approximate autocovariance model was used for all the facies:

$$C(h) = 2V_1H(2H-1)h^{2H-2} \qquad (1)$$

This is an approximation to the fractional Gaussian noise autocovariance function. Once H is known, V_1 is adjusted to make the function, Equation (1), fit the experimental autocovariance calculated from the core data.

Variance of the Difference between the Wells

The variograms and the R/S plots described above establish the autocovariance model in the vertical direction. For the horizontal direction, there is not enough data to calculate the variogram or the R/S plot. By assuming a fractal model, the same fractal exponent H, estimated from the vertical direction, is used for the horizontal direction. The only unknown in Equation (1) is the magnitude of V_1. The variance of the difference between two wells is one point on the horizontal variogram and allows calculation of V_1. From an analysis of all well pairs we can obtain V_1 for the model in the horizontal direction.

In the Schneider Field the average interwell variance is about the same as the maximum separation value for the vertical variogram. These manipulations indicate that the autocovariance function in Equation (1) applies for all directions, but in the horizontal directions h is stretched by a factor equal to the field dimensions divided by the vertical extent.

Averaging

From about 150 core samples in a well, only six layers are to be simulated. We must therefore average six groups of approximately 25 samples stacked vertically to reduce the 150 point data set to six points in each well. There are various classical methods of averaging permeabilities such as arithmetic, geometric, and harmonic averaging.[37-39] Power averaging[40] encompasses all methods with its transformation exponent p ranging from -1 to +1.

$$g_{p\text{-}av} = \left(\frac{1}{N} \sum_{I=1}^{N} g_I^p \right)^{1/p} \qquad (2)$$

Arithmetic averaging occurs when p= 1; when p= -1 the procedure results in harmonic averaging.

The method used to determine p for our work preserves the coefficient of variation, CV, of the permeabilities. CV is defined as the standard deviation divided by the mean. The CV is chosen as the criterion for two reasons. First, it is a dimensionless parameter which directly affects dispersion and other fluid flow characteristics. Second, when all permeability values are multiplied by a constant, the coefficient of variation is unchanged. This allows the effective permeability to be defined to achieve the same pressure drop as the original permeability before averaging and at the same time maintain the same degree of heterogeneity.

Application of this method requires assuming several values of p and then calculating the CV of the reduced, averaged data set. The value of p that produces a reduced data set CV equal to the original data set CV is then chosen. For the Schneider Field a value of p= -0.2 was used for log permeability.

Three Dimensional Permeability Model

A 40 by 21 by 6 layer grid system was constructed to represent the field (Figure 11). This system size provided a balance between the detail needed for reservoir description and computer limitations of storage and speed. An initial three dimensional conditional simulation was performed using only the data from the four wells (Figure 12). This model did honor the control points with comparable heterogeneity suggested by the averaged core data but did not adequately model the geological model described by the petrologist and the geologist. The four spatial control points are not sufficient to cause the mathematical process of conditional simulation to match the symmetry of the reefal depositional framework.

Specifically, the permeabilities should degrade away from the reefal core area near the Jones 2 and Jones 3 STH

to the east, southeast, south, and southwest. This is exhibited in the easterly direction by the poorer quality rock in the SASI Ranch. Sufficient well control is not available in the other directions to confirm the degree of permeability degradation suggested by the depositional environment and geological model. This problem was solved by defining a vertical surface that would be expected to contain rock quality similar to the SASI Ranch. A two dimensional conditional simulation along this surface would produce a field that can be input as control points in a final three dimensional conditional simulation.

Two Dimensional Conditional Model

The SASI Ranch is the only well to intersect the edge of the reservoir. It exhibits the poorer rock quality that the geologic model predicts toward the eastern and southern edges of the field. To better match the geologic model in the three dimensional simulation, a 48 by 6 vertical, two dimensional conditional simulation was constructed to represent the surface of poorer quality rock at the edge of the reservoir. The areal extent of the two dimensional surface is shown in Figure 11. Duplicating the SASI Ranch data at three additional points in the conditional simulation achieved better control of the model and provided a closer match to the geologic data.

Final Three Dimensional Conditional Simulation

The two dimensional conditional simulation permeability values were then used, along with three additional existing well control points, to produce a final three dimensional conditional simulation (Figure 13). In general, higher permeabilities are located in the reef core, with lower permeabilities to east and south. The final simulated model matched the predicted geological model of the field. To our knowledge, this is the first three dimensional conditional simulation that incorporates such geologic detail.

Fluid Flow Simulation

A fluid flow simulation was then generated to predict the movement of fluids through the reservoir. As predicted from the petrological study, history matching the interference test pressures required increasing the permeabilities in both the reef and reef debris facies. The in-situ reservoir scale permeabilities in these facies is greater than measured by full diameter, whole core analysis. The match was achieved by multiplying the permeabilities in these facies by a scaling factor. The technique of power averaging the measured core permeabilities by preserving the CV enables scaling the permeabilities to match pressure history, while keeping the same degree of reservoir heterogeneity.

The information produced by the fluid flow simulation is now being used to manage the current and future production of the reservoir, predict future injection requirements, and delineate the fluid flow through the formation.

Conclusions

1. Improved reservoir management results from a comprehensive data acquisition program coupled with engineering, geological, and petrological studies.

2. Successful three dimensional conditional simulation requires the incorporation of a detailed geological reservoir model that reliably projects reservoir facies beyond the wellbore.

3. The Schneider Field is developed in a Buda reef complex. Three reservoir facies have been identified: reef, reef debris, and shoaling grainstone apron.

4. The petrological study predicted that both the reef and reef debris facies in-situ permeabilities would be greater than measured by full diameter whole core analysis. This observation was confirmed by subsequent fluid flow simulation history matching.

5. Power averaging permeabilities, preserving the CV of the original distribution, enables history matching of pressure drops without reducing the heterogeneity of the reservoir model.

Nomenclature

BOPD	Barrels of oil per day
BWIPD	Barrels of water injected per day
C(h)	Autocovariance function of separation h
CV	Coefficient of variation, the mean divided by the standard deviation[20]
h	Separation (lag) distance
H	Fractal exponent

K90	Permeability measured 90 degrees to direction of maximum value
Kmax	Permeability measured in direction of maximum value
Kvert	Permeability measured in vertical direction
MSTB	Thousands of stock tank barrels
N	Number of observations to be power averaged
p	Power averaging exponent
pdf	Probability density function
RB	Reservoir barrels
R/S Plot	Rescaled range plot[26,35,36]
SCF	Standard cubic feet
STB	Stock tank barrels
STH	Side-track hole
V_1	Variogram value at h=1

Acknowledgements

We thank Energy Production Corporation for permission to publish this work. We would also like to thank Michael Fox, Sam French, and Bob Meade for their help on this project.

We also acknowledge the Enhanced Oil Recovery Research Program of the Center for Petroleum and Geosystems Engineering at The University of Texas. Larry W. Lake holds a Shell Distinguished Chair.

References

1. Nichols, E.A.: "Geothermal Gradients in Midcontinent and Gulf Coast Oil Fields," *Trans.* AIME (1947) **170**, 44-50.

2. Amyx, Bass, and Whiting, *Petroleum Reservoir Engineering*, McGraw-Hill Book Company, New York City (1960).

3. McCain, Jr. William D. *The Properties of Petroleum Fluids, 2nd Edition*, PennWell Books, Tulsa, (1990).

4. Lomando, A.J., "Aptian Depositional Patterns Influenced by Salt Tectonics, Central East Texas Basin," (Abstract) AAPG, (1980), v. 73, no. 3, 382.

5. Barker, C., "Organic Geochemistry in Petroleum Exploration," AAPG, Continuing Education Course Note Series No. 10, (1980).

6. Wendlandt, E.A, Shelby, T.H. Jr., and Bell, J.S., "Hawkins Field, Wood County, Texas," AAPG Bull. (Nov. 1946) v. 30, no. 11, 1830-1856.

7. Lee, W.J. et al, "A Mathematical Model of the Hawkins Woodbine Reservoir," JPT (Dec. 1977) 1545-1549.

8. King, R.L., and Lee, W.J., "An Engineering Study of the Hawkins (Woodbine) Field," JPT (Feb. 1976) 123-128.

9. Flugel, E., *Microfacies Analysis of Limestones*, Springer-Verlag, New York City (1982).

10. Harbour, J.L., and Mathis, R.L., "Sedimentation, Diagenesis, and Porosity Evolution of Carbonate Sands in the Black Lake Field of Central Louisiana," *Carbonate Sands - A Core Workshop*, Harris, P.M. (ed.), SEPM core workshop No. 5 (1984) 306-333.

11. Achauer, C.W., "Facies, Morphology, and Major Reservoir Controls in the Lower Cretaceous James Reef, Fairway Field, East Texas," *Carbonate Petroleum Reservoirs*, Roehl, P.O. and Choquett, P.W. (eds.), Springer-Verlag, New York City (1985).

12. Lake, L.W., and Carroll, H.B. Jr. (eds.), *Reservoir Characterization*, Academic Press, Orlando (1986).

13. Lake, L.W., Carroll, H.B. Jr., and Wesson, T.C. (eds.), *Reservoir Characterization II*, Academic Press, San Diego (1991).

14. Van De Graaff, W.J.E., and Ealey, P.J., "Geological Modeling for Simulation Studies", AAPG Bull., v. 73, no. 11 (November, 1989) 1436-1444.

15. Johnson, C.R., and Jones, T.A., "Putting Geology into Reservoir Simulations: A Three-Dimensional Modeling Approach," paper SPE 18321 presented at the 1988 Annual Technical Conference, Houston, Texas, Oct. 2-5.

16. Testerman, J.D., "A Statistical Reservoir Zonation Technique", *Trans.*, AIME (1962) **225**, 889-893.

17. Davis, John C., *Statistics and Data Analysis in Geology*, John Wiley & Sons, New York City (1973).

18. Cressie, Noel, *Statistics for Spatial Data*, John Wiley & Sons, New York City (1991).

19. Journel, A.G., and Huijbregts, Ch.J., *Mining Geostatistics*, Academic Press (1978).

20. Isaaks, E.H., and Srivastava, R.M., *Applied Geostatistics*, Oxford University Press (1989).

21. Ripley, Brian D., *Spatial Statistics*, John Wiley & Sons, New York City (1981).

22. Kelkar, Mohan, "Introduction to Geostatistics," Tutorial Paper, Third International Reservoir Characterization Technical Conference, Tulsa, Nov. 3-5, 1991.

23. Kim, Young C., *Introductory Geostatistics and Mine Planning*, Course Notes, University of Arizona Department of Mining and Geological Engineering (1990).

24. De Costa e Silva, A.J., "A New Approach to the Characterization of Reservoir Heterogeneity Based on the Geomathematical Model and Kriging Technique," paper SPE 14275 presented at the 1985 Annual Technical Conference, Las Vegas, Sept. 22-25.

25. Chopra, A.K., Severson, C.D., and Carhart, S.R., "Evaluation of Geostatistical Techniques for Reservoir Characterization," paper SPE 20734 presented at the 1990 Annual Technical Conference, New Orleans, Sept. 23-26.

26. Hewett, T.A., "Fractal Distributions of Reservoir Heterogeneity and Their Influence on Fluid Transport," paper SPE 15386 presented at the 1986 SPE Annual Technical Conference and Exhibition, New Orleans, Oct. 5-8.

27. Hewett, T.A., and Behrens, R.A., "Conditional Simulation of Reservoir Heterogeneity with Fractals," SPERE (Sept. 1990) 217-225.

28. Yang, A.P., "Stochastic Heterogeneity and Dispersion," PhD dissertation, The University of Texas Department of Petroleum Engineering (1990).

29. Mandelbrot, B.B., *The Fractal Geometry of Nature*, Freeman, New York City (1983).

30. Emanuel, A.S., Alameda, G.K., Behrens, R.A., and Hewett, T.A., "Reservoir Performance Prediction Methods Based on Fractal Geostatistics," SPERE (Aug. 1989) 311-318.

31. Matthews, J.L., Emanuel, A.S., and Edwards, K.A., "A Modeling Study of the Mitsue Stage 1 Miscible Flood Using Fractal Geometries," paper SPE 18327 presented at the 1988 Annual Technical Conference, Houston, Oct. 2-5.

32. Crane, S.D., and Tubman, K.M., "Reservoir Variability and Modeling with Fractals," paper SPE 20606 presented at the SPE 1990 Annual Technical Conference, New Orleans, Sept. 23-26.

33. Aasum, Y., Kelkar, M.G., and Gupta, S.P., "An Application of Geostatistics and Fractal Geometry for Reservoir Characterization," SPEFE (March 1991) 11-19.

34. Perez, G., and Chopra, A.K., "Evaluation of Fractal Models to Describe Reservoir Heterogeneity and Performance," paper SPE 22694 presented at the 1991 SPE Annual Technical Conference, Dallas, Oct. 6-9.

35. Mandelbrot, B.B., and Van Ness, J.W., "Fractional Brownian Motions, Fractional Noises, and Applications," SIAM Rev., Oct. 1968, 10, 4, 422-437.

36. Mandelbrot, B.B., and Wallis, J.R., "Robustness of the Rescaled Range R/S in the Measurement of Noncyclic Long Run Statistical Dependence", Water Resources Research, Oct. 1969.

37. Law, J., "Statistical Approach to the Interstitial Heterogeneity of Sand Reservoirs," *Trans.* AIME (1944) **155**, 202-222.

38. Warren, J.E., and Price, H.S., "Flow in Heterogeneous Porous Media," *Trans.* AIME (1961) **222**, 153-169.

39. Jensen, J.L., Hinkley, D.V., and Lake, L.W., "A Statistical Study of Reservoir Permeability: Distributions, Correlations, and Averages," SPERE (Dec. 1987), 461-468.

40. Journel, A.G., Deutsch, C., and Desbarats, A.J., "Power Averaging for Block Effective Permeability," paper SPE 15128 presented at the 1986 SPE California Regional Meeting, Oakland, Apr. 2-4.

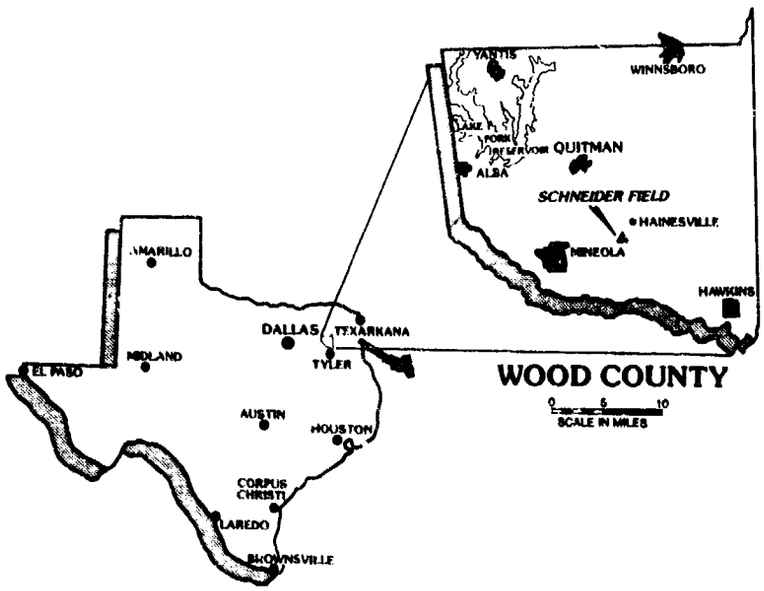

Figure 1 - Location of Schneider (Buda) Field.

Figure 2 - Rendered View of Haineaville Salt Dome and Schneider (Buda) Field Reservoir.

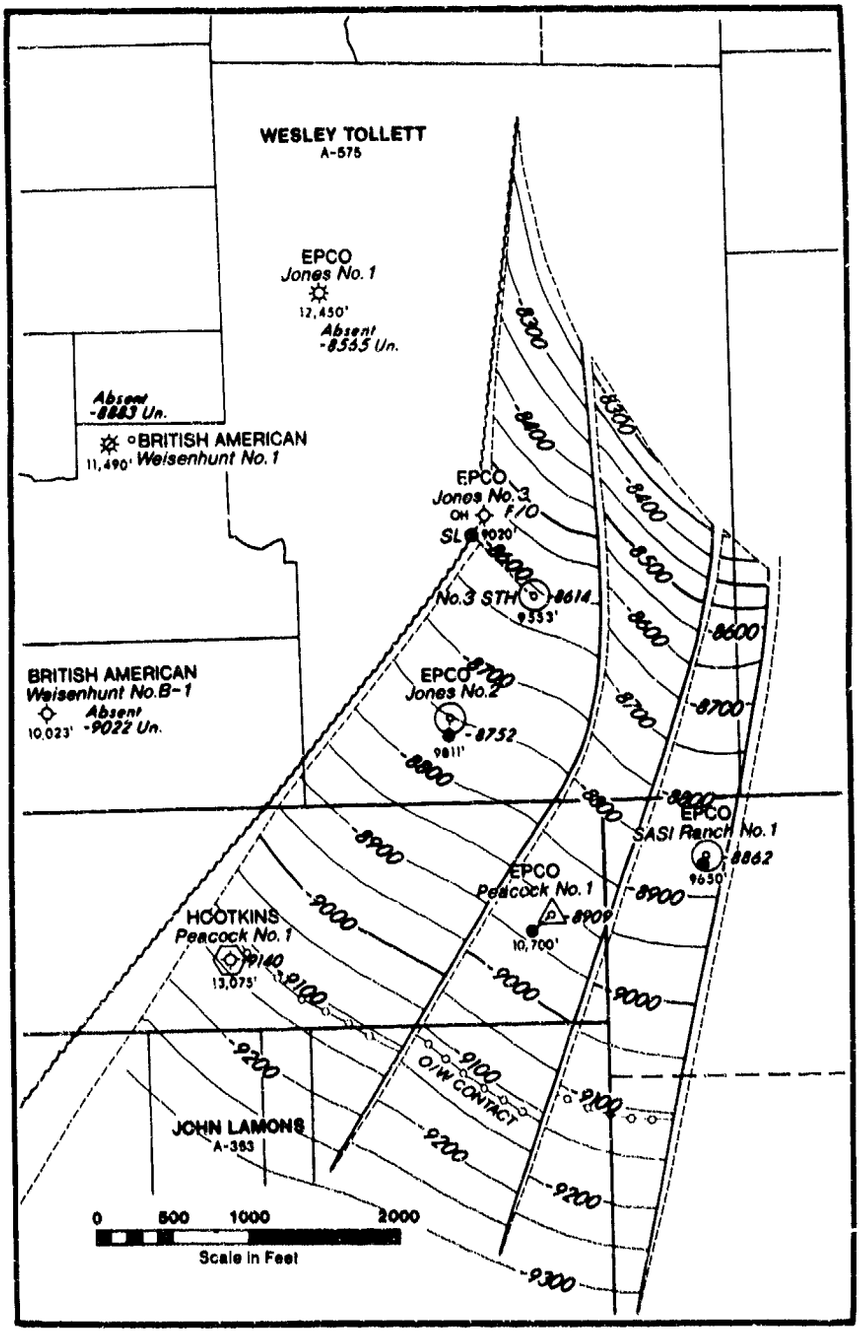

Figure 3 - Structure Map of Schneider (Buda) Field on Top of Buda Formation.

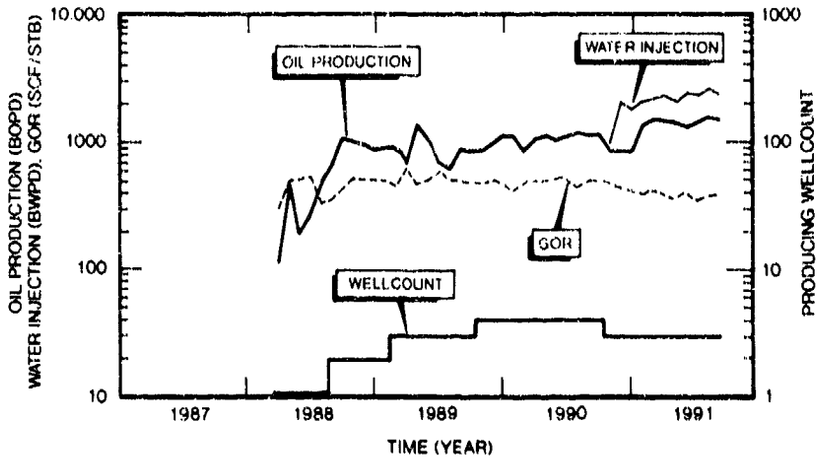

Figure 4 - Production/Injection History Graph of Schneider (Buda) Field.

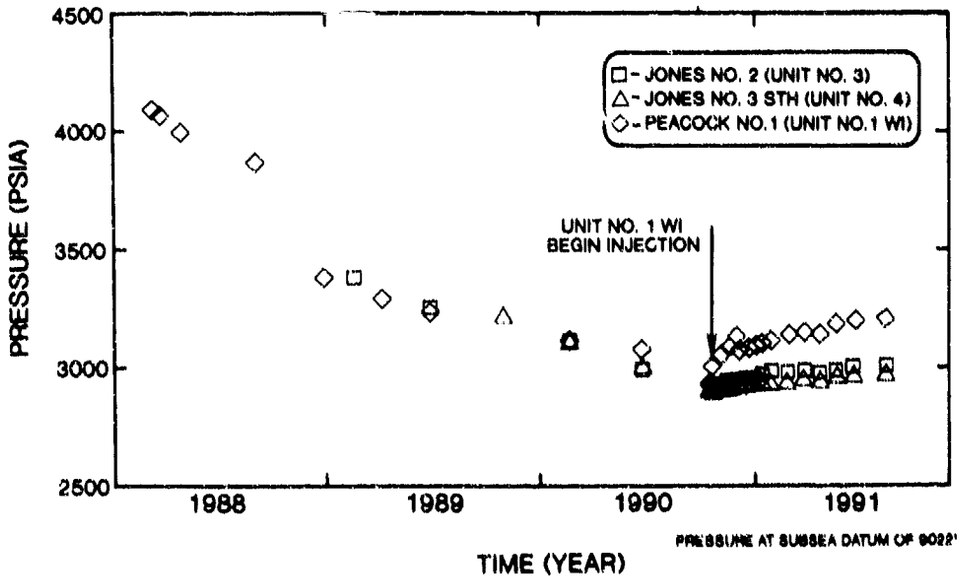

Figure 5 - Pressure History Graph of Schneider (Buda) Field.

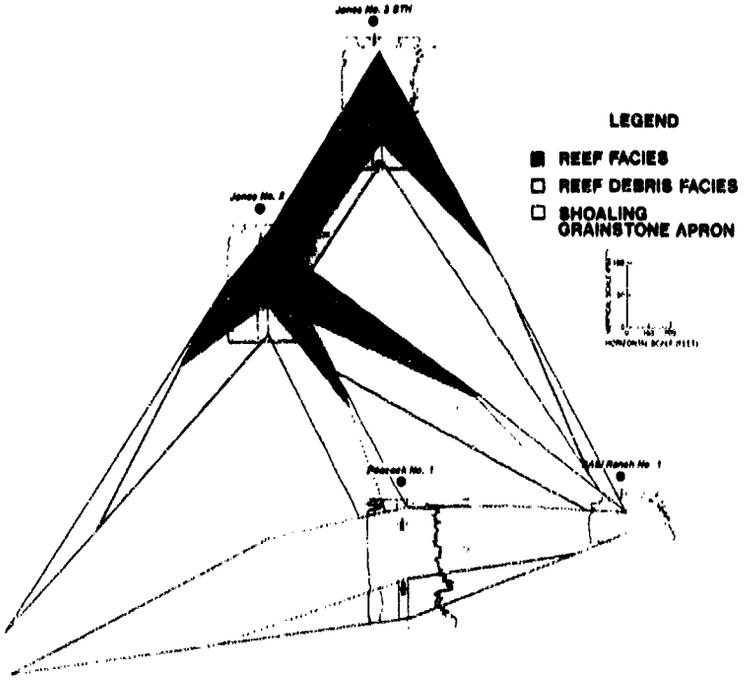

Figure 6 - Fence Diagram of Schneider (Buda) Reservoir.

Figure 7 - Rendering of Reef Debris Facies.

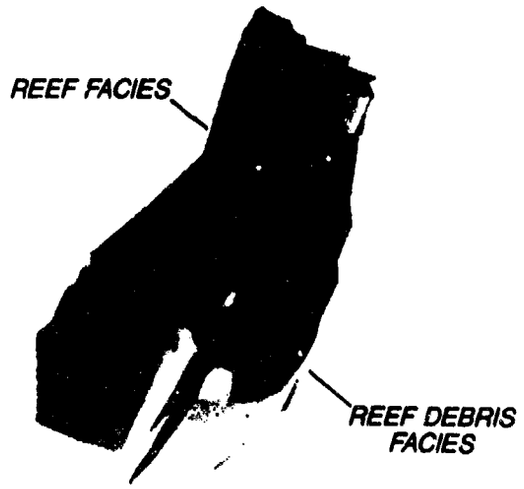

Figure 8 - Rendering of Reef and Reef Debris Facies.

Figure 9 - Rendering of all Three Facies: Reef, Reef Debris, and Shoaling Grainstone Apron.

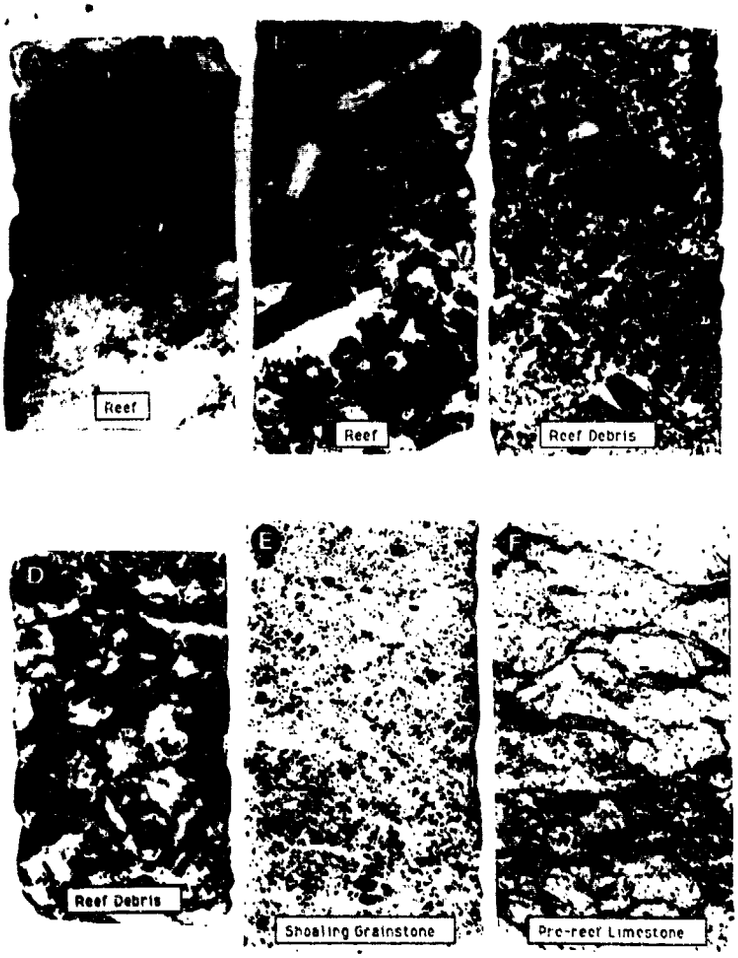

Figure 10 - Core Slab Photographs of the Four Lithofacies Present in the Schneider Field.

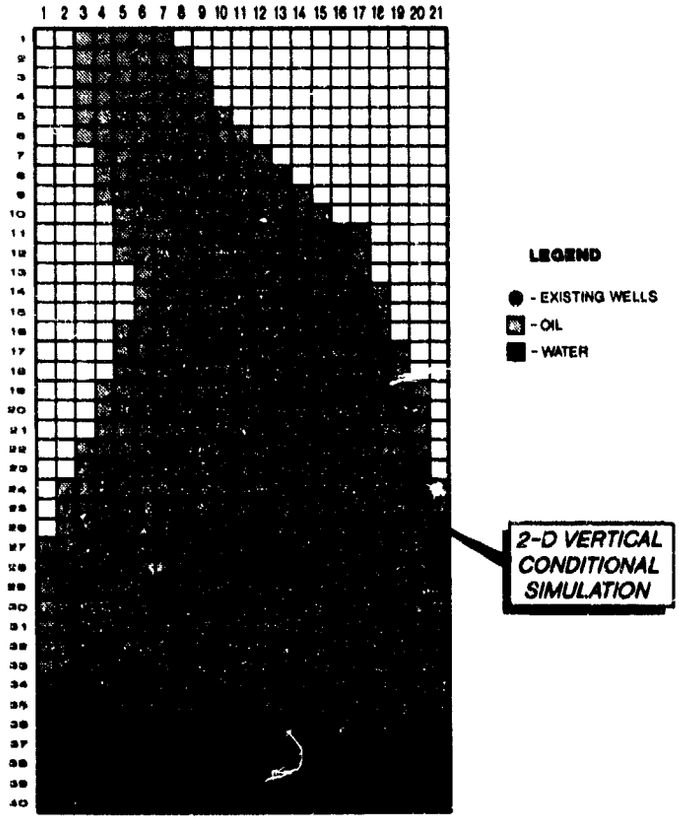

Figure 11 - Schematic of Three Dimensional Conditional Simulation Grid.

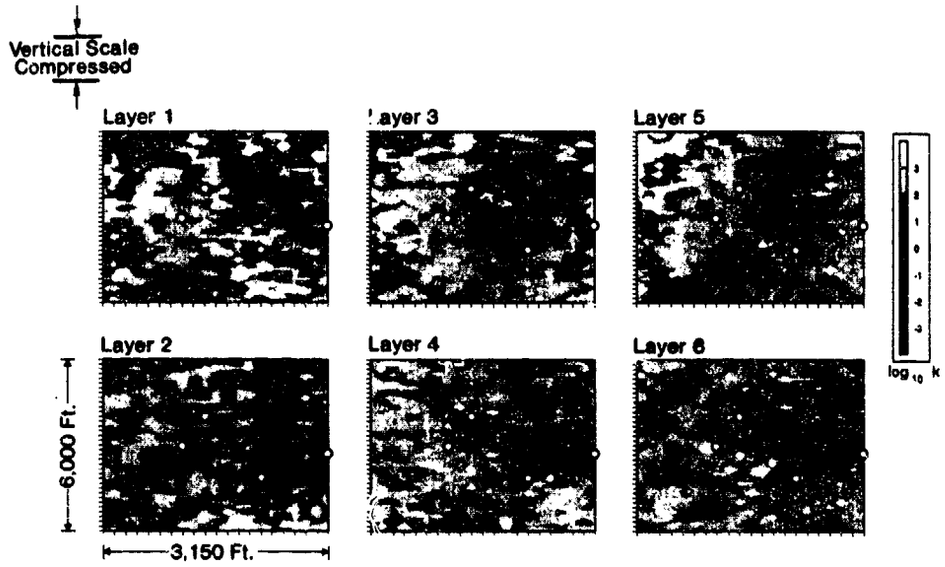

Figure 12 - First Three Dimensional Permeability Distribution.

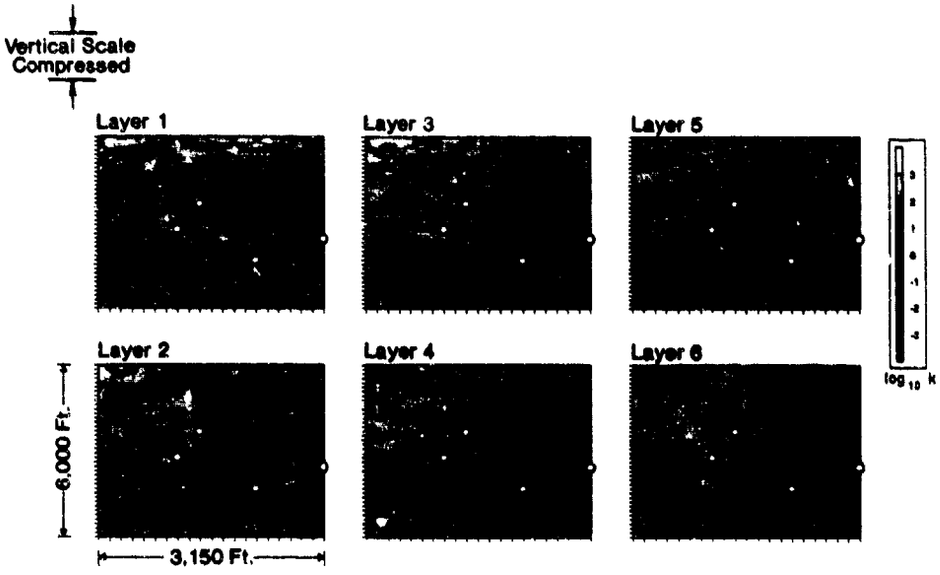

Figure 13 - Final Three Dimensional Permeability Distribution.